Monte Carlo Field-Theoretic Simulations for Melts of Symmetric Diblock Copolymer

ARTICLE *in* MACROMOLECULES · SEPTEMBER 2013

Impact Factor: 5.8 · DOI: 10.1021/ma401687j

2 AUTHORS:

Pawel Stasiak
University of Reading
14 PUBLICATIONS **127** CITATIONS
SEE PROFILE

Mark W Matsen
University of Waterloo
134 PUBLICATIONS **7,827** CITATIONS
SEE PROFILE

Macromolecules

Article

pubs.acs.org/Macromolecules

Monte Carlo Field-Theoretic Simulations for Melts of Symmetric Diblock Copolymer

P. Stasiak and M. W. Matsen[†,*]

School of Mathematical and Physical Sciences, University of Reading, Whiteknights, Reading RG6 6AX, U.K.

ABSTRACT: Monte Carlo field-theoretic simulations (MC-FTS) are performed on melts of symmetric diblock copolymer for invariant polymerization indexes extending down to experimentally relevant values of $\bar{N} \sim 10^4$. The simulations are performed with a fluctuating composition field, $W_-(\mathbf{r})$, and a pressure field, $W_+(\mathbf{r})$, that follows the saddle-point approximation. Our study focuses on the disordered-state structure function, $S(k)$, and the order−disorder transition (ODT). Although short-wavelength fluctuations cause an ultraviolet (UV) divergence in three dimensions, this is readily compensated for with the use of an effective Flory−Huggins interaction parameter, χ_e. The resulting $S(k)$ matches the predictions of renormalized one-loop (ROL) calculations over the full range of $\chi_e N$ and $\bar{N}$ examined in our study, and agrees well with Fredrickson−Helfand (F−H) theory near the ODT. Consistent with the F−H theory, the ODT is discontinuous for finite $\bar{N}$ and the shift in $(\chi_e N)_{\mathrm{ODT}}$ follows the predicted $\bar{N}^{-1/3}$ scaling over our range of $\bar{N}$.

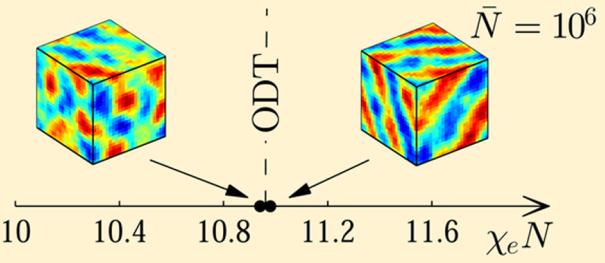

INTRODUCTION

Block copolymer melts have received considerable attention as a result of their intriguing behavior and a wide range of potential applications.[1] Our understanding of them is largely based on the pioneering works of Helfand,[2] Leibler,[3] and Semenov,[4] all of which applied mean-field theory to what has become known as the standard Gaussian chain model.[5] The partition function for a melt of AB diblock copolymer, in terms of this model, is given by

$$Z \sim \int \exp\left(\rho_0 \chi \int \hat{\phi}_{\mathrm{A}} \hat{\phi}_{\mathrm{B}} d\mathbf{r}\right) \delta[\hat{\phi}_{\mathrm{A}} + \hat{\phi}_{\mathrm{B}} - 1] \prod_{\alpha=1}^{n} P[\mathbf{r}_\alpha] \mathcal{D}\mathbf{r}_\alpha \tag{1}$$

where $\mathbf{r}_\alpha(s)$ is the space curve of the α'th chain ($\alpha = 1, 2, ..., n$ and $0 \le s \le 1$)

$$P[\mathbf{r}_\alpha] = \frac{3}{2a^2 N} \int_0^1 |\mathbf{r}'_\alpha(s)|^2 \, ds \tag{2}$$

is the Weiner weighting and

$$\hat{\phi}_{\mathrm{A}}(\mathbf{r}) = \frac{N}{\rho_0} \sum_{\alpha=1}^{n} \int_0^f \delta(\mathbf{r} - \mathbf{r}_\alpha(s)) \, ds \tag{3}$$

is a dimensionless A-segment concentration; the B-segment concentration, $\hat{\phi}_{\mathrm{B}}(\mathbf{r})$, is the same but integrated from $s = f$ to 1. The model parameters include the Flory−Huggins interaction χ, the degree of polymerization N, the diblock composition f, the total number of molecules n, the statistical segment length a, and the bulk segment density ρ_0. While mean-field theory has been extraordinarily successful in accounting for the general behavior of block copolymer melts,[5] there are some aspects that it treats poorly, in particular the disordered state and thus the order−disorder transition (ODT).

In another seminal paper by Fredrickson and Helfand (F−H),[6] it was shown that the fluctuation corrections to mean-field theory are controlled by the invariant polymerization index $\bar{N} \equiv \rho_0^{-2} a^6 N$. For symmetric ($f = 0.5$) diblock copolymers, the disordered-state structure function was predicted to vary as

$$\frac{S(k)}{\rho_0 N} = \frac{1}{F(k^2 a^2 N/6) - 2\chi N + 256.8/\sqrt{\bar{N}\tau}} \tag{4}$$

where $F(x)$ is a function derived by Leibler,[3] and $\tau \equiv \rho_0 N / S(k^*)$ satisfies

$$\tau = 2(10.495 - \chi N) + \frac{256.8}{\sqrt{\bar{N}\tau}} \tag{5}$$

As anticipated by Leibler and predicted by Fredrickson and Helfand, fluctuations destroy the mean-field critical point for symmetric diblock copolymers at $\chi N = 10.495$, and replace it by a discontinuous ODT at

$$(\chi N)_{\mathrm{ODT}} = 10.495 + 41\bar{N}^{-1/3} \tag{6}$$

where the average A-segment concentration switches abruptly from a uniform distribution of $\langle\hat{\phi}_{\mathrm{A}}(\mathbf{r})\rangle = f$ (i.e., disordered phase) to a sinusoidal profile of $\langle\hat{\phi}_{\mathrm{A}}(\mathbf{r})\rangle = f + \phi_{\mathrm{A},1}\cos(\mathbf{r}\cdot\mathbf{k}^*)$ (i.e., lamellar phase) with a finite amplitude of

$$\phi_{\mathrm{A},1} = 1.63\bar{N}^{-1/6} \tag{7}$$

Received: August 12, 2013
Revised: September 13, 2013
Published: September 30, 2013

   dx.doi.org/10.1021/ma401687j | *Macromolecules* 2013, 46, 8037−8045

In the limit $\bar{N} \to \infty$, the expressions for $S(k)$ and $(\chi N)_{ODT}$ reduce to the mean-field predictions of Leibler,[3] obtained from the random-phase approximation (RPA). In the original F−H calculation, the principle wavevector, k^*, corresponding to the maximum in $S(k)$ was fixed at the RPA value.[3] In subsequent calculations by Barrat and Fredrickson[7] and by Mayes and de la Cruz,[8] this assumption was lifted and k^* was found to decrease with increasing fluctuations (i.e., decreasing $\bar{N}$). Mayes and de la Cruz also predicted a slightly reduced coefficient of 39 for eq 6. All these calculations, however, invoke a number of stringent approximations that are only rigorously accurate for extraordinarily large invariant polymerization indexes (i.e., $\bar{N} \gtrsim 10^{10}$), although they are routinely applied to experimentally relevant molecular weights (e.g., $\bar{N} \sim 10^3-10^4$).[9]

There have been various attempts to develop a more rigorous treatment, the most notable being the recent renormalized one-loop (ROL) calculations by Morse and co-workers.[10−12] In doing so, one has to cope with an ultraviolet (UV) divergence originally identified by de la Cruz et al.[13] It results because the free energy of a short-wavelength fluctuation scales with the magnitude of the wavevector as k^{-2}, which causes the integrated free energy to diverge linearly with k in three dimensions. The amplitude of the divergence is sensitive to the composition profile of the block copolymer morphology, but fortunately in a way that is proportional to the interaction energy. Thus, the divergence can be compensated for by a reduction in the *bare* interaction parameter, χ, which is accomplished by working in terms of the effective interaction parameter

$$\chi_e = \chi\left(1 - \frac{6}{\pi^2} l\Lambda\right) \tag{8}$$

where $l \equiv 1/\rho_0 a^2$ is the packing length and Λ is the maximum wavevector or cutoff. Once the interaction strength is renormalized, the one-loop calculations produce well-defined results. The main conclusion of the ROL calculations[11] is that the F−H theory predicts $S(k)$ accurately near the ODT, but underestimates it at small $\chi_e N$. The calculations also predict a modest reduction in the peak position, k^*, which can be attributed to the intermolecular interactions. Unfortunately, ROL calculations are not easily applied to ordered phases, which prevents predictions for the ODT.

Of course the ODT can be located with simulations, but it is extremely challenging to simulate an accurate representation of the standard Gaussian chain model at large $\bar{N}$.[14] Fredrickson and co-workers[15,16] have proposed an alternative strategy particularly well-suited to large $\bar{N}$, where the particle-based polymer model is transformed to a system of fluctuating fields, $W_-(\mathbf{r})$ and $W_+(\mathbf{r})$. The partition function of the field-based model is given by

$$Z \sim \int \exp\left(\frac{H[W_-, W_+]}{k_B T}\right) \mathcal{D}W_- \mathcal{D}W_+ \tag{9}$$

where the new Hamiltonian

$$\frac{H[W_-, W_+]}{n k_B T} = -\ln Q[W_+ + W_-, W_+ - W_-] + \frac{1}{V}\int\left(\frac{W_-^2(\mathbf{r})}{\chi N} - W_+(\mathbf{r})\right) d\mathbf{r} \tag{10}$$

involves the single-chain partition function, $Q[W_A,W_B]$, for a diblock copolymer subjected to external fields, $W_A(\mathbf{r})$ and $W_B(\mathbf{r})$, acting on its A and B segments, respectively. Here $V = nN/\rho_0$ is the volume of the system. The functional integral over $W_-(\mathbf{r})$ extends from $-\infty$ to ∞ for each value of $\mathbf{r}$, while the integration over $W_+(\mathbf{r})$ is along the imaginary axis from $-i\infty$ to $i\infty$. Consequently, the Hamiltonian is a complex function, and the partition function is no longer a sum over real-valued positive Boltzmann weights. Fredrickson and co-workers handle this by performing complex Langevin field-theoretic simulations (CL-FTS). Initial studies were limited to two-dimensional melts,[17] but there have now been some recent simulations in three-dimensional space.[18] The 3D simulations, however, are limited to a single and relatively large invariant polymerization index of $\bar{N} = 5.4 \times 10^5$.

Schmid and co-workers[19] have proposed an alternative strategy where the functional integration over $W_+(\mathbf{r})$ is handled by the saddle-point approximation, in which case the partition function simplifies to

$$Z \sim \int \exp\left(\frac{H[W_-, w_+]}{k_B T}\right) \mathcal{D}W_- \tag{11}$$

where $w_+(\mathbf{r})$ is the extremum of $H[W_-,W_+]$ with respect to $W_+(\mathbf{r})$. The extremum (or saddle point) satisfies

$$-\frac{V}{Q}\frac{\mathcal{D}Q}{\mathcal{D}W_+}\bigg|_{W_+ = w_+} = 1 \tag{12}$$

which corresponds to a mean-field approximation of the incompressibility condition. As it turns out, $w_+(\mathbf{r})$ is real and thus the Boltzmann weight is positive definite, which means that the statistical mechanics can now be performed by standard Monte Carlo techniques[19,20] or with conventional Langevin simulations.[21]

The only example of Monte Carlo field-theoretic simulations (MC-FTS) that we are aware of are the original ones for ternary blends of AB diblock copolymer with A- and B-type homopolymer.[19,20] Because of the computational cost, the MC-FTS were only performed in 2D. This severely limits the quantitative significance of the simulations, due to the fact that fluctuation effects are particularly sensitive to the dimensionality of the system. Since then, however, there have been substantial improvements in the computational speed of computers as well as in the necessary numerical algorithms,[22] and consequently 3D simulations have become a realistic possibility. Here we illustrate this by performing the first ever MC-FTS in 3D, specifically for neat melts of symmetric (f = 0.5) diblock copolymer.

SIMULATION METHOD

This section describes our method for performing MC-FTS in a three-dimensional cube of volume $V = L^3$ with periodic boundary conditions. One of the main computational tasks in field-theoretic simulations is the evaluation of the single-chain partition function,

$$Q[W_A, W_B] = \int q(\mathbf{r}, 1)\, d\mathbf{r} \tag{13}$$

required for the Hamiltonian, $H[W_-,W_+]$, in eq 10. It is obtained from a partial partition function, $q(\mathbf{r},s)$, that satisfies the diffusion equation,

$$\frac{\partial}{\partial s} q(\mathbf{r}, s) = \left[\frac{a^2 N}{6}\nabla^2 - W_\gamma(\mathbf{r})\right] q(\mathbf{r}, s) \tag{14}$$

dx.doi.org/10.1021/ma401687j | Macromolecules 2013, 46, 8037−8045

with γ = A for $s < f$ and γ = B for $s > f$. The diffusion equation is integrated from s = 0 to 1, starting from the initial condition $q(\mathbf{r},0) = 1$. This is done by implementing the pseudospectral method,[23] where each increment along the contour of the chain, $\Delta s = 1/N_s$, is evaluated using operator splitting. The change in $q(\mathbf{r},s)$ due to the field is evaluated in real space, where functions of position are represented on a discrete mesh with a uniform spacing of $\Delta x = \Delta y = \Delta z = L/m$. Then a fast Fourier transform switches $q(\mathbf{r},s)$ to $q(\mathbf{k},s)$, and the change due to the Laplacian is evaluated in reciprocal space, where functions of wavevector are represented on another discrete mesh with a uniform spacing of $\Delta k_x = \Delta k_y = \Delta k_z = 2\pi/L$. An inverse transform returns the partial partition function to real space ready for the next step in s. To improve the accuracy, this procedure is supplemented with Richardson extrapolation.[24] Even still, we require up to $N_s = 64$ steps along the chain contour in order to achieve sufficient accuracy, particularly when using a relatively fine mesh (i.e., large m).

In MC-FTS, the composition field, $W_-(\mathbf{r})$, fluctuates while the pressure field, $W_+(\mathbf{r})$, follows the saddle point, $w_+(\mathbf{r})$. This requires a self-consistent field calculation at every Monte Carlo step to continually adjust the pressure field so that the mean-field approximation of the total segment concentration,

$$\phi_+(\mathbf{r}) = \frac{V}{Q}\int_0^1 q(\mathbf{r}, s)q^\dagger(\mathbf{r}, s)\,\mathrm{d}s \tag{15}$$

satisfies the incompressibility condition, $\phi_+(\mathbf{r}) = 1$. The calculation of $\phi_+(\mathbf{r})$ uses $q(\mathbf{r},s)$ plus a second partial partition function $q^\dagger(\mathbf{r},s)$, which satisfies the same eq 14 but with one side multiplied by -1. In this case, the diffusion equation is integrated in the negative s direction starting from $q^\dagger(\mathbf{r},1) = 1$. The adjustment of the pressure field is performed iteratively with Anderson mixing as implemented in ref 22. We stop the iterations once

$$\left[\frac{1}{V}\int(\phi_+(\mathbf{r}) - 1)^2\,\mathrm{d}\mathbf{r}\right]^{1/2} < \varepsilon \tag{16}$$

where an error tolerance of $\varepsilon = 10^{-3}$ is sufficient for our purposes.

Because the saddle point, $w_+(\mathbf{r})$, and therefore the resulting Hamiltonian, $H[W_-,w_+]$, are real-valued functions, the field-based model can now be simulated using conventional Monte Carlo techniques. To perform a Monte Carlo step (MCS), we first generate a random change in the composition field, $\Delta W_-(\mathbf{r})$, for which we must then determine the change in the pressure field, $\Delta w_+(\mathbf{r})$. As usual, the move is accepted or rejected based on the Metropolis criterion [i.e., the probability of acceptance is min $\{1,\exp(-\Delta H/k_BT)\}$], where the change in energy

$$\Delta H \equiv H[W_- + \Delta W_-, w_+ + \Delta w_+] - H[W_-, w_+] \tag{17}$$

is evaluated using eq 10 with

$$n = \sqrt{N}\frac{V}{a^3N^{3/2}} \tag{18}$$

A typical simulation begins with a number of MCS to equilibrate the system, followed by a further number of MCS during which statistics are collected for various observables.

As usual, the efficiency of a simulation relies on having a good selection of Monte Carlo moves. We alternate between the original real-space move used by Düchs,[20] where $\Delta W_-(\mathbf{r})$ is selected from a uniform distribution between $\pm\mathcal{A}_1$ at each mesh point $\mathbf{r}$, and a new Fourier-space move, where the independent real and imaginary parts of $\Delta W_-(\mathbf{k})$ are selected from a uniform distribution between $\pm\mathcal{A}_2[S(k)]^{1/2}$ at each wavevector $\mathbf{k}$. (Note that the Fourier components must satisfy $\Delta W_-(-\mathbf{k}) = \Delta W_-{}^*(\mathbf{k})$ due to the fact that $\Delta W_-(\mathbf{r})$ must be real.) The amplitude of the Fourier-space moves are weighted with the structure function, $S(k)$, which we evaluate using eq 4 with the effective interaction parameter, χ_e. The amplitudes, $\mathcal{A}_1$ and $\mathcal{A}_2$, are adjusted automatically during the beginning of the equilibration period to give an acceptance rate of approximately 40%, and then held fixed for the rest of the run. The inclusion of the Fourier-space move can increase the evolution to ordered phases by an order of magnitude, and without it our present study would not be feasible.

To evaluate observables for our diblock copolymer melts, we need to relate averages from the particle-based system, eq 1, to those from the field-based system, eq 9. In this particular study, we are interested in the first

$$\langle\delta\hat{\phi}_A(\mathbf{r})\rangle = \frac{\langle W_-(\mathbf{r})\rangle}{\chi N} \tag{19}$$

and second

$$\langle\delta\hat{\phi}_A(\mathbf{r})\delta\hat{\phi}_A(\mathbf{r}')\rangle = \frac{\langle W_-(\mathbf{r})W_-(\mathbf{r}')\rangle}{(\chi N)^2} - \frac{\delta(\mathbf{r}-\mathbf{r}')}{2\rho_0\chi} \tag{20}$$

moments of the A-segment concentration $\delta\hat{\phi}_A(\mathbf{r}) = \hat{\phi}_A(\mathbf{r}) - f$.[25] In an ordered phase, the first moment provides the composition profile of the morphology. In the disordered state, however, the first moment averages to zero and so we turn to the second moment, which provides us with structure function,

$$\begin{aligned}\frac{S(k)}{\rho_0 N} &= \frac{n}{V^2}\langle\delta\hat{\phi}_A(\mathbf{k})\delta\hat{\phi}_A(-\mathbf{k})\rangle \\ &= \frac{n}{(V\chi N)^2}\langle W_-(\mathbf{k})W_-(-\mathbf{k})\rangle - \frac{1}{2\chi N}\end{aligned} \tag{21}$$

corresponding to small-angle scattering experiments.[26] Note that the Fourier transform is defined by $g(\mathbf{k}) \equiv \int g(\mathbf{r})\exp(i\mathbf{k}\cdot\mathbf{r})\,\mathrm{d}\mathbf{r}$.

In order to locate the ODT, we run M simulations in parallel on separate computer-processor cores, over a sequence of interaction parameters, $\chi^{(i)}$ with i = 1, 2, ..., M, spanning the expected position of the transition. After every 10^3 MCS on each replica of the system, we attempt parallel-tempering moves[27] where a replica at $\chi^{(i)}$ is swapped with one at $\chi^{(j)}$ according to the probability

$$p_{i\leftrightarrow j} = \min\left\{1, \exp\left[\left(\frac{1}{\chi^{(i)}N} - \frac{1}{\chi^{(j)}N}\right) \times \frac{n}{V}\int([W_-^{(i)}]^2 - [W_-^{(j)}]^2)\,\mathrm{d}\mathbf{r}\right]\right\} \tag{22}$$

Here $W_-^{(i)}(\mathbf{r})$ denotes the configuration of the replica at $\chi^{(i)}$. In order to maximize the probability of acceptance, we only consider swaps between neighboring replicas (i.e., $\chi^{(i)}$ and $\chi^{(i+1)}$), and to take full advantage of the parallelization we attempt swaps between all pairs of neighboring replicas simultaneously, alternating between all odd values of i and then all even values.

To help detect the ODT, we monitor the distribution of

dx.doi.org/10.1021/ma401687j | Macromolecules 2013, 46, 8037−8045

$$\Psi \equiv \frac{1}{V^2}\max_{\mathbf{k}}[W_{-}(\mathbf{k})W_{-}(-\mathbf{k})] \tag{23}$$

at each value of $\chi^{(i)}$. The average of Ψ is similar to the maximum of $S(k)$ multiplied by $(\chi N)^2/n$, and thus it approaches zero in the thermodynamic limit (i.e., $n \to \infty$) when the system is in the disordered phase. On the other hand, it converges to a finite value for ordered phases, since $W_{-}(\mathbf{k}) \propto V$ for the wavevectors of a periodic morphology. Hence, $\langle\Psi\rangle$ serves as an ideal order parameter.

As discussed in the Introduction, we work in terms of the effective interaction parameter, χ_e, as opposed to the bare interaction parameter, χ, in order to compensate for the UV divergence. For convenience, its definition in eq 8 can be expressed as

$$\chi_e = \chi\left(1 - \frac{6\alpha m}{\pi\sqrt{\bar{N}}}\left(\frac{aN^{1/2}}{L}\right)\right) \tag{24}$$

by making the substitution $\Lambda = m\pi/L$. Note that we have included an extra factor of α in this new expression to correct for the fact that our wavevectors are summed over a cube (i.e., $|k_x|,|k_y|,|k_z| \le \Lambda$) rather than a sphere (i.e., $|\mathbf{k}| \le \Lambda$). The factor is obtained from the numerical integration of

$$\alpha \equiv \frac{1}{4\pi\Lambda}\int\frac{d\mathbf{k}}{k^2} = 1.2214 \tag{25}$$

RESULTS

Our simulations for the disordered-state structure function, $S(k)$, typically involve 5×10^5 MCS to equilibrate the system followed by up to 5×10^6 MCS for the evaluation of $\langle W_{-}(\mathbf{k})W_{-}(-\mathbf{k})\rangle$. To improve the accuracy of $S(k)$, we combine the statistics from 6 independent runs and evaluate eq 21 using a spherical average of $\langle W_{-}(\mathbf{k})W_{-}(-\mathbf{k})\rangle$. Because of the need to include small-wavelength fluctuations, the simulations are restricted to a modest box size of $L = 3.2aN^{1/2}$. Although this results in a sizable spacing between the allowed wavevectors, it does not significantly affect the shape of $S(k)$.

We begin by examining $S(k)$ at a large invariant polymerization index of $\bar{N} = 10^6$. To illustrate the UV divergence, Figure 1a plots $S(k)$ for a series of different spatial resolutions, L/m with m = 16, 24, and 32, simulated at the same bare interaction strength, $\chi N = 10$ (open symbols). As expected, the addition of short-wavelength fluctuations facilitated by increasing m causes a reduction in the peak height, $S(k^*)$, consistent with a decrease in segregation. To compensate for this, the simulations are repeated, but this time at the same effective interaction strength, $\chi_e N = 10$ (closed symbols). When evaluated this way, the curves for the three different values of m nicely collapse, implying that the UV divergence has been successfully removed. Furthermore, the collapsed simulation data agree well with the F−H (dashed curve) and ROL (solid curve) predictions, which themselves are in good agreement at this level of segregation.

Figure 1b repeats the simulations for $S(k)$ at a more relevant polymerization of $\bar{N} = 10^4$. Again the data for different m collapse when plotted at a fixed $\chi_e N$, although not quite as well as for the higher polymerization. It would be interesting to see if the convergence improves for larger m, but unfortunately this is not computationally feasible at present. Nevertheless, the curves are reasonably close together suggesting that they are approaching an asymptotic limit, and furthermore the trend

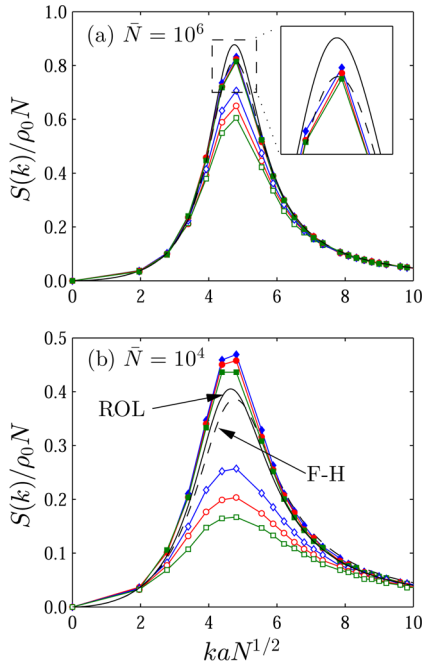

Figure 1. Disordered-state structure function, $S(k)$, simulated for invariant polymerization indexes of (a) $\bar{N} = 10^6$ and (b) $\bar{N} = 10^4$. Open and closed symbols denote results for $\chi N = 10$ and $\chi_e N = 10$, respectively, obtained using m = 16 (blue), 24 (red), and 32 (green). The F−H[6] and ROL[11] predictions are plotted with dashed and solid curves, respectively. The inset in panel a shows a magnification of the peak.

with increasing m suggests that the limit will coincide reasonably well with the ROL and F−H predictions, which are again relatively similar to each other. One important difference between the two theories, mentioned in the Introduction, is that the ROL calculations predict a shift in the peak position, k^*, toward smaller wavevectors with increasing $\bar{N}$, whereas k^* is simply held fixed in the F−H theory. Interestingly, this predicted shift in k^* is evident in the simulation results.

The $S(k)$ predicted by the simulations as well as by the F−H and ROL theories all have essentially the same shape as the RPA result of Leibler. Apart from the slight shift in k^* predicted by ROL and evident in the simulations, the only real difference among the predictions is in regards to the height of the peak, $S(k^*)$. Therefore, we now focus on the inverse of the scattering peak, for which RPA predicts $\rho_0 N/S(k^*) = 2(10.495 - \chi_e N)$. Our simulations for this are performed with m = 24, but we do run a few spot checks at m = 32 to ensure that the UV divergence remains properly accounted for by the use of $\chi_e N$. Because of the finite spacing between the allowed wavevectors, the peak of $S(k)$ is slightly truncated (see Figure 1). The resulting overestimation of $\rho_0 N/S(k^*)$ proves to be small, but nevertheless we correct for it by fitting the simulation data to a cubic spline.

Figure 2 compares our simulation results for $\rho_0 N/S(k^*)$ to the various theories. At $\bar{N} = 10^6$, everything follows the RPA prediction until $\chi_e N$ starts to approach the ODT. As emphasized by the inset of Figure 2a, the F−H and ROL calculations predict a suppression of the peak near the ODT, which is nicely captured by the simulation results. At $\bar{N} = 10^4$, however, significant differences emerge between the F−H and ROL predictions. As illustrated in Figure 2b, they still agree

dx.doi.org/10.1021/ma401687j | Macromolecules 2013, 46, 8037−8045

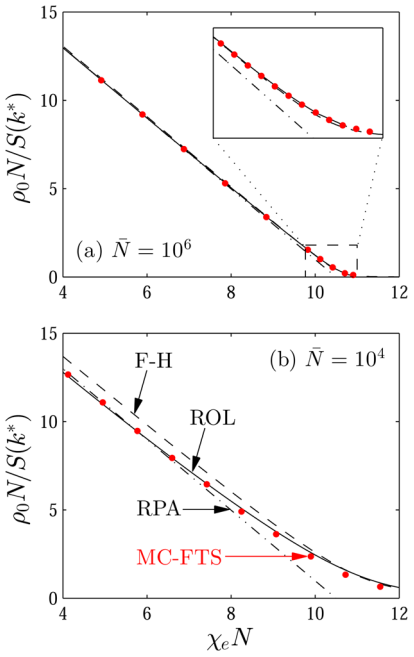

Figure 2. Inverse of the scattering peak, $1/S(k^*)$, plotted as a function of the effective segregation, $\chi_e N$, for (a) $\bar{N} = 10^6$ and (b) $\bar{N} = 10^4$. The solid dots denote simulation results using $m = 24$, while the curves compare the theoretical predictions from RPA (dash-dotted),[3] F−H (dashed),[6] and ROL (solid).[11] The inset in panel a shows a magnification of the ODT region.

near the ODT, but at lower segregations (i.e., $\chi_e N \lesssim 6$) the F−H theory predicts a significant reduction in the peak height relative to RPA whereas the ROL calculations predict a slight increase. Interestingly, the simulation results are in excellent agreement with the ROL prediction, apart from reproducing the slight enhancement of the peak at small $\chi_e N$. The MC-FTS prediction for $S(k^*)$ reduces instead to the RPA, due to the fact that the fluctuations in $W_-(\mathbf{r})$ vanish in the limit $\chi_e N \to 0$. Although the resulting inaccuracy is negligible over the present range of $\bar{N}$, the enhancement of $S(k^*)$ predicted by ROL at weak segregations does become significant for shorter polymers.[11,12]

Next we attempt to locate the ODT by simulating the order parameter, $\langle\Psi\rangle$, over a series of χN values with parallel tempering. These runs typically involve 10^6 MCS for equilibration, and a further 10^5 MCS for the collection of statistics. After some preliminary simulations, we realized that the ODT generally occurs at segregations slightly above the F−H prediction in eq 6. The position is somewhat sensitive to finite-size effects, because the period of an ordered morphology has to be commensurate with the simulation box. However, past experience[28] has shown that the lamellar structure is less affected than other morphologies, because it can select among many orientations. Nevertheless, we try to minimize the finite-size effects by choosing an appropriate box size, L, specifically $\sqrt{6}$ times the self-consistent field theory (SCFT) prediction of the equilibrium period[29] evaluated at the F−H estimate of $(\chi N)_{\mathrm{ODT}}$ from eq 6. With this choice, the lamellar phase spontaneously forms in one of the (211) orientations of the simulation box, as expected. A few simulations were repeated with slightly smaller or larger boxes to ensure that the results are not overly sensitive to our choice of L.

Figure 3a plots the order parameter as a function of χN for an invariant polymerization index of $\bar{N} = 10^6$. The three curves

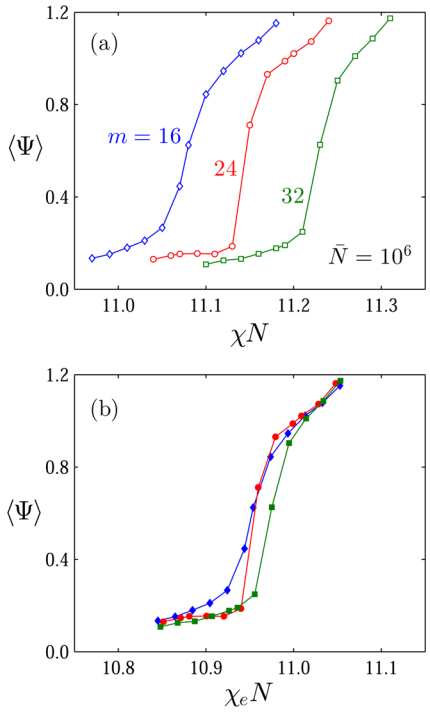

Figure 3. Order parameter, $\langle\Psi\rangle$, plotted as a function of the (a) bare χN and (b) effective $\chi_e N$ for $\bar{N} = 10^6$ with $m = 16$ (blue), 24 (red), and 32 (green).

were generated with the same $L/aN^{1/2} = 3.29$, but with different numbers of mesh points, m. The location of the ODT, which corresponds to the sharp rise in $\langle\Psi\rangle$, moves to higher χN as the spatial resolution increases (i.e., larger m), consistent with the UV divergence. Indeed, Figure 3b shows that the three curves collapse, to within our statistical error, when replotted in terms of the effective $\chi_e N$. Note that statistical errors do not result in the usual noisy curves, because the errors at different χN are correlated due to the parallel-tempering moves.

To confirm the occurrence of the ODT, it is useful to examine histograms of Ψ at each value of χN. Figure 4 plots histograms at three consecutive segregations from the parallel tempering run with $m = 24$. The histogram in panel a for $\chi N = 11.13$ has a peak at $\Psi \approx 0.15$ corresponding to disordered-like configurations, whereas the one in panel c for $\chi N = 11.17$ has a peak at $\Psi \approx 0.85$ corresponding to ordered-like configurations. The histogram at the intermediate segregation of $\chi N = 11.15$, however, exhibits two peaks at small and large Ψ from disordered and ordered configurations, respectively, implying that we are very near the ODT. This switch, where a population of configurations with small Ψ declines while a distinct population with large Ψ emerges, is a telltale signature of a discontinuous phase transition. The crossover from one population to the other will become more and more abrupt with increasing system size, V, leading to a true discontinuity in the thermodynamic limit.

As a result of the discontinuity, the lamellar phase emerges with a composition profile of finite amplitude. To illustrate this, we evaluate $\langle\hat{\phi}_{\mathrm{A}}(\mathbf{r})\rangle$ from a single replica held at a fixed segregation of $\chi N = 11.17$. This small increment above $(\chi N)_{\mathrm{ODT}} \approx 11.15$ was sufficient for the lamellar phase to

dx.doi.org/10.1021/ma401687j | Macromolecules 2013, 46, 8037−8045

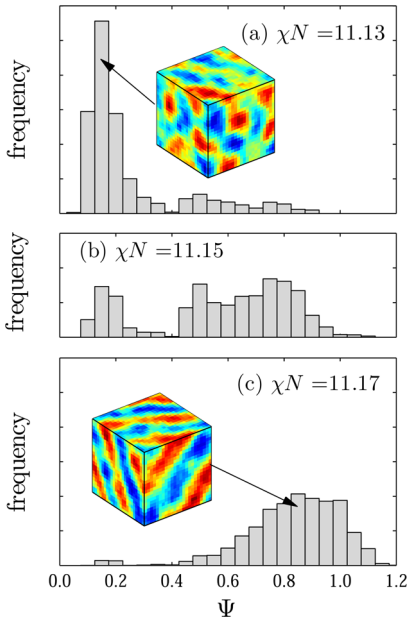

Figure 4. Histograms of Ψ generated at (a) χN = 11.13, (b) χN = 11.15, and (c) χN = 11.17 from a parallel tempering run for $\bar{N} = 10^6$ with m = 24. Typical configurations are shown for Ψ ≈ 0.15 and 0.85, corresponding to the dominant populations at χN = 11.13 and 11.17, respectively.

remain locked into a single orientation during the 7×10^6 MCS over which the statistics were collected. The volume of the system was also sufficient to prevent any noticeable translational drift of the morphology. Figure 5 projects the ensemble-

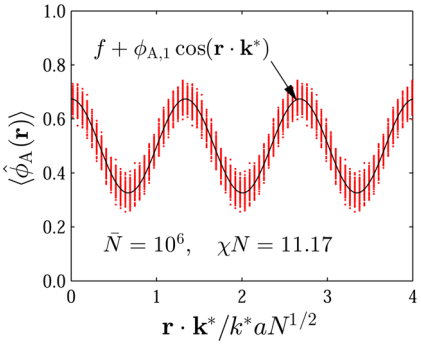

Figure 5. Composition profile, $\langle \hat{\phi}_A(\mathbf{r}) \rangle$, projected onto the direction of the dominant wavevector, $\mathbf{k}^*$, from a simulation just inside the ordered region at χN = 11.17 with $\bar{N} = 10^6$ and m = 24. The black curve shows the first-harmonic approximation obtained from $\phi_{A,1} = 2|\langle \delta\hat{\phi}_A(\mathbf{k}^*) \rangle|/V$.

averaged composition, $\langle \hat{\phi}_A(\mathbf{r}) \rangle$, onto an axis parallel to the dominant wavevector, $\mathbf{k}^*$, corresponding to the maximum of $|\langle \delta\hat{\phi}_A(\mathbf{k}^*) \rangle|$. Among the considerable spatial fluctuations in composition, as evident by the spread in the data, there are well-defined oscillations characteristic of the lamellar phase. As shown by the black curve, the oscillations are nicely captured by the first-harmonic approximation, $f + \phi_{A,1} \cos(\mathbf{r} \cdot \mathbf{k}^*)$, where the Fourier coefficient is given by $\phi_{A,1} = 2|\langle \delta\hat{\phi}_A(\mathbf{k}^*) \rangle|/V$. Interestingly, the amplitude of the composition profile, $\phi_{A,1}$ = 0.174, agrees well with the F−H prediction of $\phi_{A,1}$ = 0.163 from eq 7.

When locating the ODT, we took particular care to ensure that the system had sufficient time to equilibrate. This was done by performing two separate parallel-tempering runs with diametrically contrasting initial conditions, one where all M replicas were started with $W_-(\mathbf{r}) = 0$ and another where they were all initialized with an ordered lamellar configuration. In most cases, the two simulations converged, implying that they both reached equilibrium. However, at our lowest $\bar{N} = 10^4$, the time required to equilibrate the system in the vicinity of the ODT became exceedingly long. This is demonstrated in Figure 6, where we compare the order parameter, $\langle \Psi \rangle$, generated from

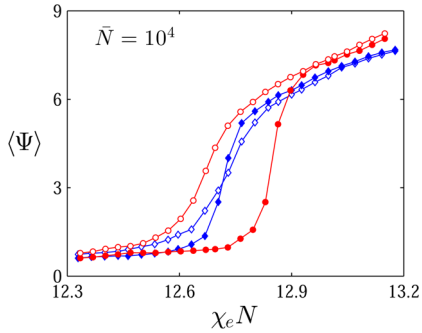

Figure 6. Order parameter, $\langle \Psi \rangle$, from parallel-tempering simulations at $\bar{N} = 10^4$ using m = 16 (blue) and 24 (red), where the replicas were all initialized with either uniform (solid symbols) or lamellar (open symbols) configurations.

the two separate simulations. The curves for m = 16 have converged to within our statistical error, but the ones for m = 24 exhibit a sizable metastability loop in the region of the ODT, which would become even wider for m = 32. This is because we have to decrease the amplitudes of the MC moves, $\mathcal{A}_1$ and $\mathcal{A}_2$, for finer meshes in order to maintain a reasonable acceptance rate, which makes it increasingly difficult for the system to overcome energy barriers. In order for the loop to narrow, individual replicas have to convert from the metastable to the stable state, which is hampered by the fact that the driving force for this becomes very small near the ODT while the discontinuity of the ODT results in a large energy barrier. The metastability loop is so persistent at $\bar{N} = 10^4$ and m = 24 that even an extra 10^6 MCS of equilibration had no appreciable effect on its width. Although this prevents us from pinpointing the ODT, we can nevertheless assume that its position is bracketed by the interval of the metastability loop.

Figure 7 shows a logarithmic plot of the fluctuation-induced shift in the ODT, $(\chi_e N)_{ODT} - 10.495$, as a function of $\bar{N}$ obtained from simulations with m = 24. Interestingly, the simulation results are consistent with the red line that runs parallel to the black line denoting the F−H prediction from eq 6. This implies that the $\bar{N}^{-1/3}$ scaling predicted by F−H theory extends to experimentally relevant polymerizations of $\bar{N} \sim 10^4$. To examine the discontinuity of the ODT, we evaluate the first harmonic of the lamellar profile, $\phi_{A,1} = 2|\langle \delta\hat{\phi}_A(\mathbf{k}^*) \rangle|/V$, immediately above $(\chi_e N)_{ODT}$ at each value of $\bar{N}$. Figure 8 shows the results plotted on a logarithmic scale, which are again consistent with F−H theory. In this case, the simulations follow the $\bar{N}^{-1/6}$ scaling of eq 7 until $\bar{N} \lesssim 10^5$. This deviation from the predicted scaling at small $\bar{N}$ is not surprising, since the amplitude of the composition profile cannot increase indefinitely; after all, it has an upper limit of $\phi_{A,1} \approx 0.5$.

dx.doi.org/10.1021/ma401687j | Macromolecules 2013, 46, 8037−8045

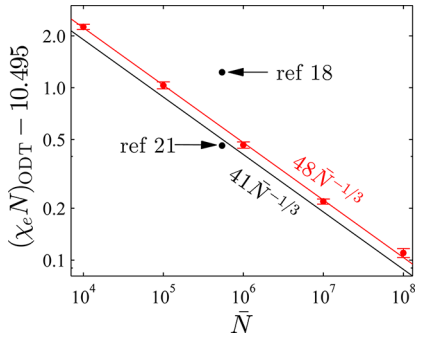

Figure 7. Fluctuation correction to the ODT, $(\chi_e N)_{ODT} - 10.495$, plotted on a logarithmic scale as a function of the invariant polymerization index, $\bar{N}$. The red line is a fit to the simulation data and the black line is the F−H prediction from eq 6. The black dots denote previous FTS results from refs 18 and 21.

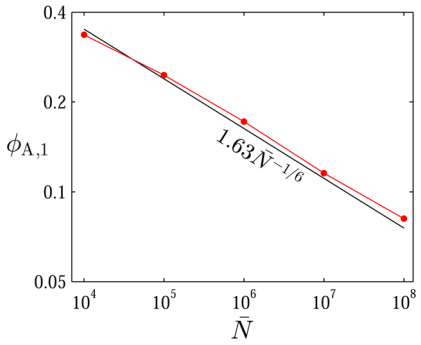

Figure 8. Principle harmonic of the lamellar profile, $\phi_{A,1} = 2|\langle\delta\hat{\phi}_A(\mathbf{k}^*)\rangle|/V$, at the ODT plotted on a logarithmic scale as a function of the invariant polymerization index, $\bar{N}$. The black line denotes the F−H prediction from eq 7.

DISCUSSION

The main motivation for this study was to test the feasibility of extending the Monte Carlo field-theoretic simulations (MC-FTS) introduced a decade ago by Düchs and Schmid[19,20] from $d = 2$ to $d = 3$ dimensions, which is crucial for quantitative predictions given the strong effect dimensionality has on fluctuations. In this regard, the study has been very encouraging. We have been able to obtain accurate statistics over a wide range of invariant polymerization indexes (i.e., $\bar{N} = 10^4-10^8$) with modest computing resources. Even after years of development by Fredrickson and co-workers, the application of the alternative complex Langevin field-theoretic simulations (CL-FTS) to $d = 3$ has, so far, been limited to a single and relatively large $\bar{N} = 5.4 \times 10^5$.[18] Although it is too premature to suggest that MC-FTS are more effective than CL-FTS, they are certainly competitive and worthy of further investigation.

It is important to remember, however, that the MC-FTS are, in principle, less accurate because they apply the saddle-point approximation to the pressure field, $W_+(\mathbf{r})$, responsible for enforcing incompressibility, $\hat{\phi}_+(\mathbf{r}) = 1$. Nevertheless, we expect the composition field, $W_-(\mathbf{r})$, to fluctuate far more than $W_+(\mathbf{r})$, and thus the approximation seems completely appropriate. Indeed, initial comparisons found excellent agreement between MC-FTS and CL-FTS,[19] and a subsequent more detailed examination concluded that the saddle-point approximation is highly accurate.[21] This conclusion should be taken with a degree of caution though, as it is based on 2D simulations with a relatively large Ginzburg parameter, $C \equiv \rho_0 R_g^d/N = 50$, which is equivalent to $\bar{N} = 5.4 \times 10^5$ for $d = 3$. (Note that N does not control the size of fluctuation effects when $d = 2$.) For a more relevant comparison, there are two previous 3D Langevin simulations performed at $C = 50$, which located the ODT with and without the saddle-point approximation. In this case, however, there is a considerable discrepancy between their respective values of $(\chi_e N)_{ODT} = 11.0$ and 11.6 for the bulk ODT of symmetric diblock copolymers, denoted by solid dots in Figure 7.[30] While the estimate obtained by Alexander-Katz and Fredrickson[21] using the saddle-point approximation agrees reasonably well with our results, the fluctuation-induced shift of the ODT predicted by the CL-FTS of Lennon et al.[18] is nearly twice as large. This suggests that the saddle-point approximation is less accurate in 3D for some reason, but the discrepancy might also just be a result of computational inaccuracy. This will need further investigation.

Our field-theoretic simulations are the first to demonstrate the compositionally dependent UV divergence expected for the standard Gaussian chain model.[10,11,13] For $d = 2$, one should observe a slow logarithmic divergence, and so it is not surprising that it was not detected in the earlier 2D simulations.[17,19] The previous 3D CL-FTS of Lennon et al.[18] did report a UV divergence, but no dependence on composition was detected implying that it could be ignored by simply fixing the cutoff, Λ, at a sufficiently large value. The composition dependence may have been overlooked because the simulations were performed with parameters for which χ_e and χ only differed by 4%. In contrast, χ_e and χ differ by about 30% for our $\bar{N} = 10^4$ simulations.

It is surprising that the renormalization of the interaction parameter, given by eq 8, works so well when χ_e and χ differ by so much. Grzywacz et al.[10] argued that extending the loop expansion for dense polymer melts to include terms beyond one loop would produce divergences proportional to higher powers of $l\Lambda$. Therefore, the renormalization is expected to fail as $l\Lambda$ becomes of order unity. The fact we do not encounter this problem suggests that the saddle-point approximation for $W_+(\mathbf{r})$ tames the UV divergence, which is a very advantageous side effect.

In addition to the effective reduction in χ, the UV divergence is predicted to cause an effective increase in the statistical segment length.[10,31] This results from enforcing the incompressibility condition, $\hat{\phi}_+(\mathbf{k}) = 0$, for all nonzero wavevectors up to the cutoff, Λ.[31] As a consequence, the domains of a block copolymer morphology should increase in size, which would manifest itself in Figure 1 as a horizontal shift of $S(k)$ toward smaller wavevectors with increasing m. Just as with χ, this could be compensated for by renormalizing a, or in other words by replotting $S(k)$ as a function of $ka_eN^{1/2}$, where a_e is an effective statistical segment length. However, this shift in a is absent from our MC-FTS, presumably because they apply the saddle-point approximation rather than strictly enforcing the incompressibility condition. The effect should still occur in the CL-FTS, although it has not yet been reported.

The disordered-state structure function, $S(k)$, has been evaluated using FTS before, but our results are far more accurate. In the previous simulations by Alexander-Katz and Fredrickson,[21] structure functions were generated for films of diblock copolymer. Although their thickest films should have exhibited bulk behavior, their choice of system parameters led to relatively poor resolution, the absolute intensities were not determined and the constant term in eq 21 was neglected. Consequently, we are the first to provide meaningful

dx.doi.org/10.1021/ma401687j | Macromolecules 2013, 46, 8037−8045

comparisons with the competing theories. It is particularly satisfying that our simulations agree so remarkably well with the ROL calculations, clearly confirming the improvement over the F−H predictions. In light of the discrepancy with the CL-FTS[18] noted above, the agreement with ROL provides valuable evidence that the saddle-point approximation is in fact reliable.

The fluctuation-induced shift of the ODT predicted by Fredrickson and Helfand, eq 6, has become a well-accepted result that is often used to determine the temperature dependence of χ.[32] However, there has never been any real evidence that the $\bar{N}^{-1/3}$ scaling remains accurate down to the values of $\bar{N}$ to which it is typically applied. Müller and Daoulas[14] have suggested that it does, but their evidence is not particularly compelling as it comes from comparing distinctly different simulations in order to span a sufficient range of $\bar{N}$. Contrary to this, CL-FTS simulations by Ganesan and Fredrickson[17] found a significant deviation from the predicted F−H scaling for $C \lesssim 125$, which would correspond to $\bar{N} \lesssim 3 \times 10^6$ in 3D. This finding, however, was only for 2D simulations. Our results, on the other hand, now provide compelling evidence that the $\bar{N}^{-1/3}$ scaling holds to much smaller Ginzburg parameters in 3D, reaching experimentally relevant polymerizations of at least $\bar{N} \sim 10^4$. Although we find a larger fluctuation-induced shift of the ODT corresponding to a coefficient of 48 (see Figure 8), this small deviation from the F−H theory could possibly be due to computational inaccuracies.

We have certainly obtained useful quantitative predictions from these initial 3D MC-FTS, but it would be nice to push the simulations to smaller $\bar{N}$ and to improve the accuracy. To do so, we would have to deal with the considerable metastability near the ODT for small $\bar{N}$, but this could be accomplished by employing alternative MC techniques such as Wang−Landau sampling[33] or thermodynamic integration to obtain the free energy.[18] It may also be possible to perform a finite-size scaling analysis with such methods. If we are to improve accuracy and obtain better resolution in $\mathbf{k}$, it will be necessary to consider larger system sizes and possibly finer mesh resolutions. Some of the computational demands could be met by massive parallelization using graphics processing units (GPUs).[34] It would also be useful to explore alternative MC moves. Although our simulations were greatly accelerated by the introduction of a new Fourier-space move, we still needed millions of MCS per simulation and even more would be required for larger systems. Any improvements in these directions would also have the added benefit of extending the range of systems to which the MC-FTS could be applied.

SUMMARY

This study investigated fluctuation effects in melts of symmetric ($f = 0.5$) diblock copolymer using Monte Carlo field-theoretic simulations (MC-FTS)[19,20] applied to the standard Gaussian chain model. The simulations were performed in three dimensions, and for invariant polymerization indexes extending down to an experimentally relevant value of $\bar{N} = 10^4$. The UV divergence expected in three dimensions due to short-wavelength fluctuations was observed as the spatial resolution was increased. Fortunately, this effect could be compensated for by renormalizing the interaction parameter as specified by eq 24. There was no need to renormalize the statistical segment length, because the saddle-point approximation used in MC-FTS relaxes the incompressibility condition.

In terms of $\chi_e N$, the simulations produced well-behaved predictions for the disordered-state structure function, $S(k)$, relatively independent of the spatial resolution. Furthermore, the results were consistent with the recent renormalized one-loop (ROL) calculations of Qin et al.[11] In particular, the height of the peak, $S(k^*)$, closely followed the mean-field random-phase approximation (RPA) until close to the ODT, where it was then suppressed by fluctuations. The simulations also showed evidence for a slight shift in k^* toward smaller wavevectors near the ODT with increasing fluctuations (i.e., smaller $\bar{N}$), consistent with the ROL calculations.

Our simulations located the ODT, $(\chi_e N)_{\mathrm{ODT}}$, over a wide range of invariant polymerization indexes, $\bar{N}$, by examining an order parameter, $\langle \Psi \rangle$, over a sequence of $\chi_e N$ values using parallel tempering. The discontinuity of the ODT was demonstrated by examining histograms of Ψ and the average concentration profile, $\langle \hat{\phi}_{\mathrm{A}}(\mathbf{r}) \rangle$. At the ODT, the histograms exhibited a bimodal distribution indicating a clear distinction between disordered and ordered configurations, while the concentration jumped from a uniform profile to a sinusoidal profile of finite amplitude, $\phi_{A,1}$. For our smallest $\bar{N} = 10^4$, the discontinuity of the ODT prevented the system from fully equilibrating, but nevertheless we could bracket the position of the ODT by examining the metastability of the competing phases. The dependence of $(\chi_e N)_{\mathrm{ODT}}$ on $\bar{N}$ was found to agree remarkably well with the Fredrickson-Helfand (F−H) prediction in eq 6, but with a slightly larger coefficient. This provides the first compelling evidence that the $\bar{N}^{-1/3}$ scaling holds down to values of $\bar{N}$ characteristic of real experiments. Furthermore, the discontinuity of the ODT was in good agreement with the F−H prediction in eq 7.

The feasibility of MC-FTS in three-dimensional space was made possible by the inclusion of a Fourier-space Monte Carlo move and the use of advanced numerics developed for self-consistent field theory (SCFT), where the diffusion equation is solved with a fourth-order pseudospectral method and the field equations are satisfied by Anderson mixing. There is still considerable scope for further improvements, such as the use of more sophisticated MC techniques, massive parallelization with GPUs, and the inclusion of more efficient MC moves. This would allow for improved accuracy, permit larger scale simulations, and facilitate applications to more complicated systems. After a decade of inactivity following its introduction, the outlook for MC-FTS now appears very promising.

AUTHOR INFORMATION

Corresponding Author

*(M.W.M.) E-mail: mwmatsen@uwaterloo.ca.

Present Address

†Institute for Nanotechnology, University of Waterloo, Waterloo, Ontario N2L 3G1, Canada

Notes

The authors declare no competing financial interest.

ACKNOWLEDGMENTS

We are grateful to Dave Morse and Friederike Schmid for useful discussions, and to Jen Glaser for providing the ROL predictions. This work was supported by a grant from the EPSRC (U.K.) and computing resources from the SHARCNET facility (University of Waterloo).

REFERENCES

(1) Bates, F. S.; Fredrickson, G. H. *Phys. Today* **1999**, *52*, 32−38.
(2) Helfand, E. *J. Chem. Phys.* **1975**, *62*, 999−1005.
(3) Leibler, L. *Macromolecules* **1980**, *13*, 1602−1617.
(4) Semenov, A. E. *Sov. Phys. JETP* **1985**, *85*, 733−742.
(5) Matsen, M. W. *J. Phys.: Condens. Matter* **2002**, *14*, R21−R47.
(6) Fredrickson, G. H.; Helfand, E. *J. Chem. Phys.* **1987**, *87*, 697−705.
(7) Barrat, J.-L.; Fredrickson, G. H. *J. Chem. Phys.* **1991**, *95*, 1281−1289.
(8) Mayes, A. M.; de la Cruz, M. O. *J. Chem. Phys.* **1991**, *95*, 4671−4677.
(9) Bates, F. S.; Schulz, M. F.; Khandpur, A. K.; Förster, S.; Rosedale, J. H.; Almdal, K.; Mortensen, K. *Faraday Discuss.* **1994**, *98*, 7−18.
(10) Grzywacz, P.; Qin, J.; Morse, D. C. *Phys. Rev. E* **2007**, *76*, 061802.
(11) Qin, J.; Grzywacz, P.; Morse, D. C. *J. Chem. Phys.* **2011**, *135*, 084902.
(12) Qin, J.; Morse, D. C. *Phys. Rev. Lett.* **2012**, *108*, 238301.
(13) de la Cruz, M. O.; Edwards, S. F.; Sanchez, I. C. *J. Chem. Phys.* **1988**, *89*, 1704−1708.
(14) Müller, M.; Daoulas, K. C. *J. Chem. Phys.* **2008**, *128*, 024903.
(15) Fredrickson, G. H.; Ganesan, V.; Drolet, F. *Macromolecules* **2002**, *35*, 16−39.
(16) Fredrickson, G. H. *Soft Matter* **2007**, *3*, 1329−1334.
(17) Ganesan, V.; Fredrickson, G. H. *Europhys. Lett.* **2001**, *55*, 814−820.
(18) Lennon, E. M.; Katsov, K.; Fredrickson, G. H. *Phys. Rev. Lett.* **2008**, *101*, 138302.
(19) Düchs, D.; Ganesan, V.; Fredrickson, G. H.; Schmid, F. *Macromolecules* **2003**, *36*, 9237−9248.
(20) Düchs, D. Dissertation, Universität Bielefeld: 2003.
(21) Alexander-Katz, A.; Fredrickson, G. H. *Macromolecules* **2007**, *40*, 4075−4087.
(22) Stasiak, P.; Matsen, M. W. *Eur. Phys. J. E* **2011**, *34*, 110.
(23) Rasmussen, K. Ø.; Kalosakas, G. *J. Polym. Sci., Part B* **2002**, *40*, 1777−1783.
(24) Ranjan, A.; Qin, J.; Morse, D. C. *Macromolecules* **2008**, *41*, 942−954.
(25) Müller, M.; Schmid, F. In *Advanced Computer Simulation Approaches for Soft Matter Sciences II*; Holm, C., Binder, K., Eds.; Springer-Verlag: Berlin, Germany, 2005.
(26) Matsen, M. W. In *Soft Matter: Polymer Melts and Mixtures*; Gompper, G., Schick, M., Eds.; Wiley-VCH: Weinheim, Germany, 2006.
(27) Earl, D. J.; Deem, M. W. *Phys. Chem. Chem. Phys.* **2005**, *7*, 3910−3916.
(28) Beardsley, T. M.; Matsen, M. W. *Eur. Phys. J. E* **2010**, *32*, 255.
(29) Matsen, M. W.; Bates, F. S. *Macromolecules* **1996**, *29*, 1091−1098.
(30) Based on the reported mesh resolutions, the effective interaction parameter is $\chi_e \approx 0.96\chi$.
(31) Wang, Z.-G. *Macromolecules* **1995**, *28*, 570−576.
(32) Maurer, W. W.; Bates, F. S.; Lodge, T. P.; Almdal, K.; Mortensen, K.; Fredrickson, G. H. *J. Chem. Phys.* **1998**, *108*, 2989−3000.
(33) Wang, F.; Landau, D. P. *Phys. Rev. Lett.* **2001**, *86*, 2050−2053.
(34) Delaney, K. T.; Fredrickson, G. H. *Comput. Phys. Commun.* **2013**, *184*, 2102−2110.